Design, Synthesis, *in silico* Study and Preliminary Cytotoxic Evaluation of New N-(Benzimidazol-2-yl-methyl) Benzamide Derivatives as Possible Tyrosine Kinase Inhibitors

Suhair Q. Al-Sultan[a, b*], Mohammed Hassan Mohammed[a] and Wamidh H. Talib[c]

[a]*Department of Pharmaceutical Chemistry, College of Pharmacy, University of Baghdad, Baghdad 10047, Iraq*
[b]*Baghdad Alkarkh Health directorate/ Ministry of Health; Baghdad 10011, Iraq*
[c]*Faculty of Allied Medical Sciences, Applied Science Private University, Amman 11931, Jordan*

DOI: 10.60988/p.v36i4.58

KEYWORDS:
N- (benzimidazole-2-ylmethyl) benzamide derivatives; cytotoxicity study; in-silico study; dual tyrosine kinase inhibitors

ARTICLE INFO:
Received: June 11,2024
Revised: August 19, 2024
Accepted: September 1, 2024
Available on line: January 3, 2025

*** CORRESPONDING AUTHOR:**
Suhair Q. Al-Sultan, E-mail: sohair.qasem1100e@copharm.uobaghdad.edu.iq

ABSTRACT

Receptor tyrosine kinases (RTKs) are expressed in high level in cancer cells making their targeting a justifiable strategy. Unfortunately, multiple molecular mechanisms of resistance had been identified, leading to drug resistance and toxicity, which increase the need to discover new structural tyrosine kinase inhibitors. In current study, a series of N-(benzimidazole-2-yl-methyl) benzamide derivatives were designed and docked virtually, then were synthesized, characterized, and studied preliminary structure-activity relationship for their cytotoxic activities against two cancer cell lines (breast, T47D, and lung cancer, A549) as well as Vero normal cells, using gefitinib as a reference standard. Then molecular dynamic simulation and ADME study for the most cytotoxic compound (4f) were done. According to the spectral analysis, all designed compounds were synthesized precisely. The cytotoxic studies revealed that most of the synthesized compounds were active against the T47D breast cancer cell line but felt beyond gefitinib, while only one compound (4f) was active against the A549 lung cancer cell line. More interestingly, all synthesized compounds were inactive against normal cells. Docking scores, molecular dynamic simulation as well as ADME studies of the compound (4f) gave good results. All these findings indicate that the compound (4f) is considered a good candidate for further pharmacological studies as a tyrosine kinase inhibitor (TKI).

1. Introduction

One in six fatalities globally are attributed to cancer, a global health issue. An estimated 19.3 million new instances of cancer and almost 10 million cancer-related deaths occurred worldwide in 2020. In fact, treating cancer has been a highly complex process,[1] and according to the World Health Organization (WHO), three major cancer types in 2022: lung, breast, and colorectal cancers are the leading cause of death in cancer population patients. Currently, it is clear that conventional therapies such as chemotherapy and radiotherapy are failed to cure certain types of malignancies which explain the high mortality rates that were registered in recent decades.[2] One of the most prevalent cancers, especially among women after postmenopausal age, is breast cancer that is treated according to the stage and molecular types of individual cancer.[3] It had been shown that dysregulation of kinase signaling pathways play a crucial role in both initiation and progression of many types of cancer cells.[4] For instance, the Human Epidermal Growth Factor Receptor-2 (HER2) kinase is activated in aggressive breast cancer subtypes and is linked to a poor prognosis.[5] Epidermal Growth Factor Receptor (EGFR) is frequently mutated and overexpressed in different types of human cancers (mostly lung and breast cancer and glioblastoma) and is the target of multiple cancer therapies currently adopted in clinical practice. [6-7] Monoclonal antibodies and small-molecule tyrosine kinase inhibitors (TKIs) are two clinically important pharmacological approaches in anti-EGFR therapies. [8] Protein kinase inhibitors (PKIs) are chemically varied, low-molecular-weight hydrophobic heterocycles with a molecular weight of less than 600 Da, examples: imatinib, erlotinib, and gefitinib, all of which are ATP-competitive and clinically approved. [9] TKIs have significant advantages over traditional chemotherapeutic agents, including high efficiency, low toxicity, and high specificity.[10] Unfortunately, many TKIs develop resistance during therapy, leading to a poor clinical prognosis. The most important one is the development of secondary mutations in the oncogenic kinase that abrogate the inhibitory activity of the drug, and the other is HER2 amplification, which increased ErbB2 protein abundance and was detected in a cell line model of acquired resistance to EGFR TKI.[11,12]

The ATP-binding site is conventionally partitioned into five regions: adenine is buried deep into the binding site and forms two hydrogen bonding interactions with the binding site. The ribose sugar binds to a 'ribose binding pocket.' The triphosphate chain lies along a cleft towards the enzyme surface and interacts with two metal ions and amino acids. An empty hydrophobic pocket lies opposite the ribose binding pocket. The gatekeeper residue is an amino acid situated at the entrance to the hydrophobic pocket, and the size of the residue and the nature of amino acids in the binding pockets are important to drug design. [15] Interestingly, EGFR and HER2 share a very similar kinase domain sequence (≈80% homology). Consequently, they have a very similar ATP-binding site architecture except for key amino acid differences (the glycine-rich region of the αC-helix in HER2) that explain the high flexibility of this region, the lower stability of its active conformation and the immediate accessibility of the back hydrophobic pocket, compared with EGFR, which adapts "in conformation" that is stabilized by hydrogen bonding of amino acids between the αC-helix and αE-helix. [16]

Dual-target inhibitors of EGFR and HER2 have been observed to have superior therapeutic efficacy in comparison to single-target inhibitors, and they usually bind to the "out conformation" of EGFR with αC-helix out to access the large hydrophobic pocket. 17 For example, lapatinib, which is composed of a core scaffold that serves as the hinge binder and carries two hydrophobic groups interacting with the selectivity pockets, one of which extends into the back pocket (allosteric pocket) and the other with a solubilizing group that extends into the solvent-accessible region, **Figure 1** below compares the structural requirements between mono (type I) and dual (type ½) TKIs. [18-19]

The design of new anticancer therapies focuses on the design of new derivatives of existing drugs to overcome adverse side effects and resistance to current treatments, opening up new anticancer therapies. [20]

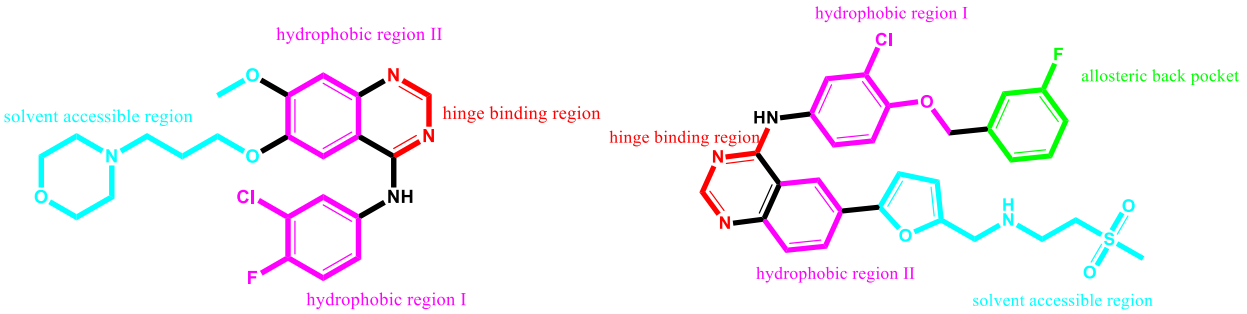

Figure 1: *Structural requirements of dual EGFR/HER2 inhibitor: lapatinib (right structure) compared with gefitinib (left structure) type I inhibitor* [19]

Benzimidazole is an isostere of purine nucleosides, so it is widely used as a basic nucleus in the development of different anticancer agents and has been widely employed as a template for synthesizing kinase inhibitors.[21-24]

In our study, we designed compounds with a benzimidazole nucleus that are as dual EGFR/HER2 inhibitors as possible, as shown in **Figure 2**.

A rational new design of dual EGFR-HER2 TKIs is based on the replacement of the quinazoline moiety (core scaffold) of the most popular TKIs by 2-(aminomethyl)benzimidazole with two nitrogen atoms of imidazole and an amine group that provide hydrogen bonding with a hinge binding region as well as the benzene ring, which represents the hydrophobic interaction. Similar to gefitinib, the solvent-accessible group was developed with a morpholine moiety, but instead of a N-alkyl (tertiary amine) group, it had a N-amide group. In order to interact with allosteric binding sites such as dual EGFR-HER2 TKIs, the other hydrophobic region was engineered to extend another hydrophobic component of various derivatives.

Next, using the Molecular Operating Environment (MOE), these structures were docked with both EGFR and HER2 proteins that had been obtained from the Protein Data Bank (PDB), and then they were synthesized and characterized precisely. Using the T47D breast cancer cell line, the A549 lung cancer cell line, and the Vero normal cell line, the cytotoxic activity of the synthesized compounds was assessed. Gefitinib was used as the reference standard. The best chemical (4f), which had the highest biological activity and good docking results, was further investigated for its toxicity and drug-likeness using molecular dynamic simulation (MDS) and ADME investigations.

2. Materials and Methods

All chemicals and reagents used in chemical synthesis were obtained from suppliers: Merck (Germany), Santa Cruz Biotechnology (Germany), Scharlau (Spain), Riedel-Dehaen (Germany), Biosolve (Netherlands), Thomas-Baker (India), Hawan (China). Thin-layer chromatography was achieved using 0.2 mm pre-coated TLC-sheets Alugram® Xtra SIL G/UV254 (Macherey-Nagel, Germany), and the visualization was under a 254 nm UV lamp. Melting points were measured using Stuart SMP3 melting point apparatus (UK) and then corrected. The Attenuated total reflection infrared (ATR-IR) was done using Shimadzu IRAffinity-1 Spectrometer (Shimadzu, Japan) and Specac® Quest ATR- diamond type (Specac Ltd., Kent, UK) at Baghdad University /college of pharmacy. 1H-NMR and 13C-NMR analysis was performed at 500 MHz and 125 MHz, respectively (d6-DMSO as the solvent) using Bruker 500 MHz-Avance III, Germany, at the University of Jordan/Faculty of Science/Department of Chemistry. Mass spectroscopy (Electrospray Ionization) ESI using High-Resolution Mass Spectrometer Buker Daltonic APEX IV, Germany, at the University of Jordan/Faculty of Science/Depart-

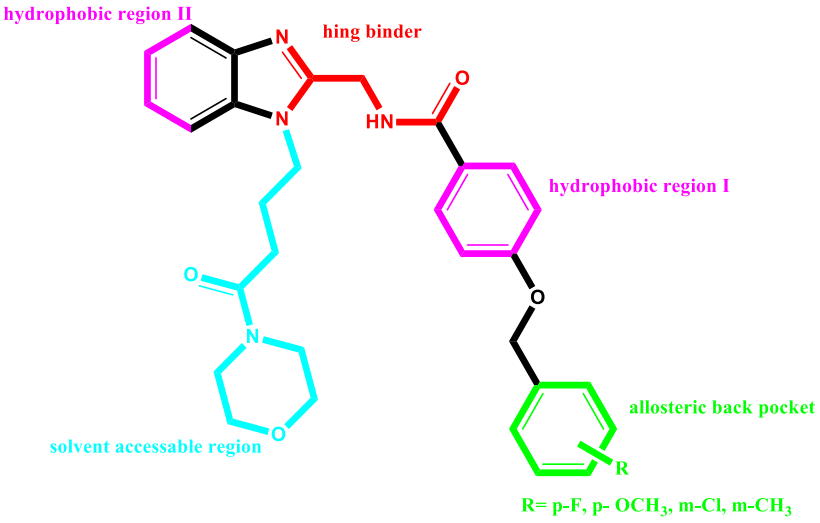

Figure 2: *Structure-activity relationship of newly synthesized compounds as possible dual TKIs*

ment of Chemistry. Molecular docking studies were performed using Molecular Operating Environment (MOE) software version 2014 (Chemical Computing Group, Montreal, Canada). While, molecular dynamic simulation was done with Maestro v 13.0.135 interface (Schrodinger, New York, NY, 2021) at Baghdad University /College of Pharmacy.

The cytotoxic assay was performed at Applied Science Private University/ Faculty of Allied Medical Sciences using three cell lines: Human alveolar cell carcinoma (A549), human breast cancer cells (T47D), and normal cell line: Vero cells (from the kidney of an African green monkey). Their incubation procedure needs 10% heat-inactivated fetal bovine serum (Gibco, UK), 1% penicillin-streptomycin (Sigma, USA), 1% L- glutamine (Sigma, USA), and 0.1% gentamycin (EuroClone, Italy). T47D cells were cultured using a complete RPMI 1640 medium (PAN-biotech, Germany), while a complete MEM medium (PAN-biotech, Germany) was used to culture A549 and Vero cells.

2.1. Chemical Synthesis

The target compounds were synthesized by multi-step reaction as shown in (Scheme1)

2.1.1. The general procedure of O- alkylation and synthesis of ethyl 4-(benzyloxy)benzoate derivatives (1a-4a):

[25] 1 mmol (0.166g) of ethyl 4-hydroxybenzoate was stirred with 3 mmol (1.25g) of anhydrous K2CO3 in 20 ml of acetonitrile for 15 min. 1.5 mmol of a meta-substituted benzyl halide derivative was added, and both were reflexed for 15hr with TLC every 3 hours. After that, the solvent was evaporated in a rotary evaporator, then iced water was added to the mixture, and the precipitate was filtered, dried, and washed with petroleum ether many times, then collected without recrystallization.

2.1.2. Ester hydrolysis and synthesis of 4-(benzyloxy)benzoic acid derivatives compounds (1b-4b):

[26] To every 1 mmol of ethyl 4-(benzyloxy)benzoate derivative, a mixture of 1 ml of tetrahydrofuran, 2ml of methanol and 1 ml of 20% NaOH solution was added, and all were stirred for 1 hour at 50oC. After the evaporation of organic solvents in a rotary evaporator, water was added to dissolve the salt, and the solution was acidified with HCl to precipitate the corresponding carboxylic acid. The precipitate was dried and washed with hot diethyl ether to get a pure carboxylic acid derivative.

2.1.3. General Synthesis of *N*-((*1H*-benzo[*d*]imidazol-2-yl)methyl)-4-(benzyloxy)benzamide derivatives (1c-4c):[27-29] In a conical flask, 2 mmol of both N-Ethyl-N′-(3-dimethylaminopropyl)carbodiimide hydrochloride (EDC.HCl) (0.38g) and 1-hydroxy benzotriazole (HOBt) (0.27g) were added to a solution of 1 mmol of 4-(benzyloxy)benzoic acid derivatives in 20 ml of dry DMF with stirring at R.T. for 3-12 hr with TLC monitoring till the conversion of all the acid to the activated ester. After cooling the solution to 0 °C, a solution of 1.5 mmol of 1H-benzimidazole-2-methylamine in 5 ml dry DMF was dropped into the activated ester, then the mixture was stirred at room temperature for 30 min to 1 hour. According to the TLC, the reaction was terminated by the addition of iced distilled water to precipitate the resulting amide derivative that was filtered, dried, and recrystallized with absolute ethanol.

2.1.4. Synthesis of ethyl 4-(2-((4-(benzyloxy)benzamido)methyl)-*1H*-benzo[*d*]imidazole-1-yl)butanoate derivatives (1d-4d):[30] A mixture of 1 mmol of compound (1c or 2c) with 2 mmol (0.276g) of anhydrous K2CO3 in 25 ml of dry acetone was stirred at room temperature for 15 min. A prepared solution of 1.5 mmol of ethyl 4-bromobutanoate with 2 mmol (0.35g) of KI in 10ml dry DMF was added to the stirred mixture, which was then reflexed at 80-90 °C for 12-24 hours with TLC monitoring. After completion of the reaction, the acetone was evaporated in a rotary evaporator. Iced water was added to precipitate the product, which was collected, dried, and washed again with HCL and then with hot water. Finally, the dried compound was recrystallized with 70% ethanol.

2.1.5. Ester hydrolysis and synthesis of 4-(2-((4-(benzyloxy)benzamido)methyl)-*1H*-benzo[*d*]imidazole-1-yl)butanoic acid derivatives (1e-4e):[26] 1 mmol of ethyl 4-(2-((4-benzyloxy)benzamido)methyl)-1H-benzo[d]imidazole-1-yl)butanoate derivative was dissolved in a mixture of 1 ml of tetrahydrofuran and 2 ml of methanol, then 1 ml og 20% NaOH solution was added and the mixture was stirred for 6 hours at room temperature. The organic solvents were evaporated, and water was added with stirring until the mixture was dissolved, then acidified by diluted HCl to precipitate the carboxylic acid that was filtrated and washed with water. The precipitate was dried and recrystallized with ethanol.

2.1.6. Synthesis of 4-(benzyloxy)-*N*-((1-(4-morpholino-4-oxobutyl)-*1H*-benzo[*d*]imidazole-2-yl)methyl)benzamide derivatives (1f-4f):[31-32] In a 100 ml conical flask, 20 ml of dry DMF with 1 mmol of one of the previous derivatives (1e-4e) was dissolved with 1.5 mmol of EDC (0.28g) and equivalent mmol of HOBt (0.2g). The solution was cooled to 0-5 °C, then 1.5 mmol (0.15g) of DMAP was added followed by a slow addition of 10 mmol (1.4ml) of TEA with 2 mmole (0.18ml) of morpholine and stirring for 1 hour at 5 °C. Then the mixture was stirred at R.T. for 24-48 hours. At the end of the reaction, crushed ice was poured into the mixture and the precipitate was collected, washed with water and finally dried to be recrystallized from 70% ethanol.

2.2. In Vitro Cytotoxicity Study

2.2.1. Maintenance of Cell Cultures:[33] Three cell lines (human breast cancer cells (T47D), human alveolar cell carcinoma (A549), and Vero cells as normal cells) were used to evaluate the antiproliferative activity of the newly synthesized compounds. The cells were cultured in a complete tissue culture medium supplemented with 10% heat-inactivated fetal bovine serum, 1% penicillin-streptomycin, 1% L-glutamine, and 0.1% gentamycin. All cells were incubated under 37 °C, 5% CO_2, and 95% humidity using a CO_2 incubator.

2.2.2. Antiproliferative Assay:[33] The MTT (3-(4,5-dimethylthiazol-2-yl)-2,5-diphenyltetrazolium bromide) test was used for testing the cytotoxicity of the designed compounds by determining the viability of prepared developing cells. This colorimetric assay is based on the reduction of yellow tetrazolium salt to purple formazan crystals by metabolically active cells. The cells were counted

and planted onto 96-well tissue culture flat-bottom microplates with 10,000 cells per well. Then, 200 µL of growth media was added and incubated for 24-hours. After seeding and monolayer formation, the medium was withdrawn.

In the present study, cells were treated with increasing concentrations (1.5–200 µM) of each compound as well as gefitinib as a positive control and incubated for 48 hours. The percentage survival was calculated using equation (1):

Percentage of cell viability (%) = (OD of treated cell/OD of negative control) ×100 (1)

where OD is the optical density.

The half-maximum inhibitory concentration (IC50) of the treated cells was determined using SPSS (Statistical Package for the Social Science, Illinois version 24).

2.3. In Silico Study

2.3.1. Molecular Docking: The chemical structures of the designed compounds were drawn using the Molecular Operating Environment (MOE) 2014 builder; then their energies were minimized. The co-crystallized ligand TAK-285 was rocked with two proteins (3RCD; HER2 and 3POZ; EGFR downloaded from PDB) after many processing steps, starting from protein preparation to pharmacophore adjustment to validate the force field applied during the docking process. Then, the prepared compounds were docked with both proteins. After completion of the docking runs, the scores of enzyme-ligand free energies of binding were obtained. The best pose of ligand binding is indicated by the lowest free energy (ΔG). The Ki (inhibitory constant) of each compound with lower energy was calculated using equation (2):[34,35]

$$Ki = e^{\Delta G}/RT \quad (2)$$

where ΔG is the binding free energy (kcal. Mol^{-1}), R is the gas constant (1.987 $cal.Mol^{-1}.K^{-1}$), and T is the absolute temperature (298.15 K).

2.3.2. Molecular Dynamic Simulation (MDS): The proteins were considered rigid during the docking performance. Therefore, to get a more realistic picture of the protein and ligand interactions, we chose and exposed one optimal complex for MDS using the Desmond module version 2.0 (academic version) according to the docking study. The system was designed by inserting a TIP3P water model in an orthorhombic periodic box of dimension 10 A^0 with an OPLS4 force field, then neutralizing it with counterions (Na+ and Cl-) at neutral pH. In various constrained steps, the built protein-ligand complex with the solvent system was maintained for energy minimization and pre-equilibration. MDS were inspected for 50 ns with 3POZ and 20 ns with 3RCD at a constant temperature of 300 K with a relaxation time of 2 ps in an NPT ensemble with a Nose-Hoover thermostat. Electrostatic interactions were treated using the Particle Mesh Ewald method for long and short range (cut-off distance of 9.0 Å), with a 10–9 tolerance limit. [36]

2.3.3. ADME study: ADME prediction was done by using the Swiss Institute of Bioinformatics website, which allows us to compute physicochemical descriptors and predict absorption, distribution, metabolism, and elimination (ADME) parameters and other pharmacokinetic properties of newly designed compounds.[37] The candidate compound subjected to this study was the 4f compound only with respect to gefitinib as a reference. By sketching their structures within the layout builder, they would be converted to smiles and then run for calculation.

3. Results and Discussion

3.1. Chemical Synthesis: According to **Scheme 1** which illustrates the overall synthesis of compounds (1f-4f), all the synthesized compounds were analyzed using different physical and advanced chemical identification methods, and all the results are mentioned as follows:

3.1.1. Ethyl 4-(benzyloxy)benzoate derivatives, compounds (1a-4a):

Compound 1a: White crystal, yield 92%, m. p. 55-

57°C. FT-IR (ATR; 1/ λ, cm^{-1}): 3070 (CH aromatic), 2989 (asym. CH2), 2870 (sym. CH2),1701(ester C=O), 1604,1512 (aromatic C–C). 1H NMR (500 MHz, DMSO) δ 7.89 – 7.83 (m, 2H), 7.47 (dd, J = 8.5, 5.6 Hz, 2H), 7.18 (t, J = 8.8 Hz, 2H), 7.09 – 7.03 (m, 2H), 5.11 (s, 2H), 4.22 (q, J = 7.1 Hz, 2H), 1.25 (t, J = 7.1 Hz, 3H).

Compound 2a: White crystal, yield 96%, m. p. 62-63 °C. FT-IR (ATR; 1/ λ, cm^{-1}): 3090 (CH aromatic), 2981(asym. CH2), 2897 (sym. CH2),1701 (ester C=O), 1604,1512 (aromatic C–C). 1H NMR (500 MHz, DMSO) δ 7.85 (d, J = 8.4 Hz, 2H), 7.34 (d, J = 8.2 Hz, 2H), 7.05 (d, J = 8.4 Hz, 2H), 6.90 (d, J = 8.2 Hz, 2H), 5.04 (s, 2H), 4.22 (q, J = 7.1 Hz, 2H), 3.70 (s, 3H), 1.25 (t, J = 7.1 Hz, 3H).

Compound 3a: White crystal, yield 86%, m. p. 40-42°C. FT-IR (ATR; 1/ λ, cm^{-1}): 3055 (CH aromatic), 2904 (asym. CH2), 2866 (sym. CH2),1701(ester C=O), 1606,1581 (aromatic C–C). 1H-NMR (500 MHz, DMSO) : 7.90 – 7.84 (m, 2H), 7.49 (s, 1H), 7.43 – 7.33 (m, 3H), 7.08 (d, J = 8.7 Hz, 2H), 5.16 (s, 2H), 4.22 (q, J = 7.1 Hz, 2H), 1.25 (t, J = 7.1 Hz, 3H).

Compound 4a: White crystal, yield 85%, m. p. 43-45 °C. FT-IR (ATR; 1/ λ, cm^{-1}): 2981 (CH aromatic), 2927(asym. CH2), 2870 (sym. CH2),1708(ester C=O), 1604,1581 (aromatic C–C). 1H-NMR (500 MHz, DMSO) : 7.86 (d, J = 8.8 Hz, 2H), 7.26 – 7.16 (m, 3H), 7.10 (d, J = 7.3 Hz, 1H), 7.08 – 7.03 (m, 2H), 5.09 (s, 2H), 4.22 (q, J = 7.1 Hz, 2H), 2.27 (s, 3H), 1.26 (d, J = 7.0 Hz, 3H).

3.1.2. 4-(benzyloxy)benzoic acid derivatives, (1b-4b):

Compound 1b: White powder, yield 95%, m. p214-216 °C. FT-IR (ATR; 1/ λ, cm^{-1}): 3055 (CH aromatic), 3100- 2546 (OH carboxylic acid), 1674 (aromatic acid C=O), 1604,1577and 1512 (aromatic C–C). 1H NMR (500 MHz, DMSO) δ 12.59 (s, 1H), 7.85 (d, J = 8.7 Hz, 2H), 7.46 (dd, J = 8.4, 5.6 Hz, 2H), 7.18 (t, J = 8.8 Hz, 2H), 7.04 (d, J = 8.7 Hz, 2H), 5.11 (s, 2H).

Compound 2b: White powder, yield 95%, m. p. 192-194 °C. FT-IR (ATR; 1/ λ, cm^{-1}): 3066 (CH aromatic), 3100- 2549 (OH carboxylic acid), 1670 (aromatic acid C=O), 1604,1577and 1512 (aromatic C–C). 1H NMR (500 MHz, DMSO) δ 12.56 (s, 1H), 7.83 (d, J = 8.7 Hz, 2H), 7.34 (d, J = 8.4 Hz, 2H), 7.06 – 7.00 (m, 2H), 6.93 – 6.87 (m, 2H), 5.04 (s, 2H), 3.71 (s, 3H).

Compound 3b: White powder, yield 96%, m. p193-195 °C. FT-IR (ATR; 1/ λ, cm-1): 3066 (CH aromatic), 3070- 2546 (OH carboxylic acid), 1678 (aromatic acid C=O), 1608,1577and 1512 (aromatic C–C). 1H-NMR (500 MHz, DMSO) : 12.65 (s, 1H), 7.85 (d, J = 8.5 Hz, 2H), 7.48 (s, 1H), 7.38 (s, 2H), 7.42 – 7.33 (m, 1H), 7.05 (d, J = 8.5 Hz, 2H), 5.15 (s, 2H).

Compound 4b: White powder, yield 94%, m. p. 163-164 °C. FT-IR (ATR; 1/ λ, cm-1): 3066 (CH aromatic), 3070- 2561(OH carboxylic acid), 1674 (aromatic acid C=O), 1604,1577and 1512 (aromatic C–C). 1H-NMR (500 MHz, DMSO) : 12.59 (s, 1H), 7.84 (d, J = 8.4 Hz, 2H), 7.21 (p, J = 7.6 Hz, 3H), 7.10 (d, J = 7.4 Hz, 1H), 7.04 (d, J = 8.4 Hz, 2H), 5.08 (s, 2H), 2.27 (s, 3H)

3.1.3. *N*-((*1H*-benzo[*d*]imodazol-2-yl)methyl)-4-(benzyloxy)benzamide derivatives, (1c-4c):

Compound 1c: White powder, yield 68%, m. p 207-210 °C. FT-IR (ATR; 1/ λ, cm^{-1}):3275 (N-H secondary amide), 3066 (CH aromatic), 1631 (C=O amide),1608 (C=N benzimidazole), 1578, 1539 and 1512 (aromatic C–C). 1H NMR (500 MHz, DMSO) δ 12.16 (s, 1H), 8.98 (t, J = 5.7 Hz, 1H), 7.88 (d, J = 8.6 Hz, 2H), 7.47 (dd, J = 8.4, 5.6 Hz, 2H), 7.44 (s, 2H), 7.18 (t, J = 8.8 Hz, 2H), 7.12 – 7.03 (m, 4H), 5.12 (s, 2H), 4.62 (d, J = 5.7 Hz, 2H).

Compound 2c: White powder, yield 77%, m. p. 222-224 °C. FT-IR (ATR; 1/ λ, cm^{-1}): 3278 (N-H secondary amide), 3012 (CH aromatic), 1639 (C=O amide),1608 (C=N benzimidazole), 1573, 1546 and 1504(aromatic C–C). 1H NMR (500 MHz, DMSO) δ 12.15 (s, 1H), 8.96 (t, J = 5.8 Hz, 1H), 7.86 (d, J = 8.5 Hz, 2H), 7.43 (s, 2H), 7.34 (d, J = 8.3 Hz, 2H), 7.12 – 7.01 (m, 4H), 6.90 (d, J = 8.5 Hz, 2H), 5.04 (s, 2H), 4.62 (d, J = 5.7 Hz, 2H), 3.71 (s, 3H).

Compound 3c: White powder, yield 96%, m. p206-208 °C. FT-IR (ATR; 1/ λ, cm^{-1}):3305 (N-H secondary amide), 3101 (NH benzimidazole), 3047 (CH aromatic), 1643 (C=O amide),1604 (C=N benzimidazole), 1573, 1550and 1504 (aromatic C–C). 1H-NMR (500 MHz, DMSO) : 12.14 (s, 1H), 8.97 (t, J = 5.8 Hz, 1H), 7.87 (d, J = 8.6 Hz, 2H), 7.49 (s, 2H), 7.42 – 7.32

(m, 3H), 7.35 (s, 1H), 7.11 – 7.04 (m, 4H), 5.16 (s, 2H), 4.62 (d, J = 5.7 Hz, 2H).

Compound 4c: White powder, yield 91%, m. p. 199-200 °C. FT-IR (ATR; 1/ λ, cm^{-1}): 3278 (N-H secondary amide), 3111 (NH benzimidazole), 3055 (CH aromatic), 1643 (C=O amide),1608 (C=N benzimidazole), 1573, 1548 and 1508 (aromatic C–C). 1H-NMR (500 MHz, DMSO) : 12.15 (s, 1H), 8.96 (t, J = 5.8 Hz, 1H), 7.87 (d, J = 8.7 Hz, 2H), 7.47 (s, 1H), 7.39 (s, 2H), 7.27 – 7.17 (m, 4H), 7.11 – 7.02 (m, 3H), 5.09 (s, 2H), 4.62 (d, J = 5.7 Hz, 2H), 2.27 (s, 3H)

3.1.4. Ethyl 4-(2-((4-(benzyloxy)benzamido) methyl)-*1H*-benzo[*d*]imidazole-1-yl)butanoate derivatives (1d-4d):

Compound 1d: White powder, yield 71%, m. p130-132 °C. FT-IR (ATR; 1/ λ, cm^{-1}):3294 (N-H secondary amide), 3062 (CH aromatic), 1720 (C=O ester),1624(C=O amide),1604 (C=N benzimidazole), 1539 and 1504 (aromatic C–C). 1H NMR (500 MHz, DMSO) δ 8.95 (t, J = 5.6 Hz, 1H), 7.84 (d, J = 8.8 Hz, 2H), 7.55 – 7.43 (m, 4H), 7.22 – 7.09 (m, 4H), 7.03 (d, J = 8.6 Hz, 2H), 5.10 (s, 2H), 4.70 (d, J = 5.6 Hz, 2H), 4.25 (t, J = 7.6 Hz, 2H), 3.95 (q, J = 7.1 Hz, 2H), 2.31 (t, J = 7.3 Hz, 2H), 1.92 (p, J = 7.4 Hz, 2H), 1.08 (t, J = 7.1 Hz, 3H).

Compound 2d: White powder, yield 76%, m. p. 131-133 °C. FT-IR (ATR; 1/ λ, cm^{-1}): 3294 (N-H secondary amide), 3050 (CH aromatic), 1732 (C=O ester),1620 (C=O amide),1604 (C=N benzimidazole), 1535 and 1504 (aromatic C–C). 1H NMR (500 MHz, DMSO) δ 8.94 (t, J = 5.6 Hz, 1H), 7.83 (d, J = 8.5 Hz, 2H), 7.52 (t, J = 8.2 Hz, 2H), 7.34 (d, J = 8.3 Hz, 2H), 7.16 (dt, J = 28.5, 7.4 Hz, 2H), 7.01 (d, J = 8.5 Hz, 2H), 6.90 (d, J = 8.4 Hz, 2H), 5.03 (s, 2H), 4.70 (d, J = 5.6 Hz, 2H), 4.25 (t, J = 7.6 Hz, 2H), 3.95 (q, J = 7.1 Hz, 2H), 3.70 (s, 3H), 2.31 (t, J = 7.3 Hz, 2H), 1.92 (p, J = 7.4 Hz, 2H), 1.08 (t, J = 7.1 Hz, 3H).

Compound 3d: White powder, yield 90%, m. p136-138 °C. FT-IR (ATR; 1/ λ, cm^{-1}):3309 (N-H secondary amide), 3050 (CH aromatic), 1724 (C=O ester),1627 (C=O amide),1608 (C=N benzimidazole), 1547 and 1508 (aromatic C–C). 1H-NMR (500 MHz, DMSO) : 8.96 (t, J = 5.6 Hz, 1H), 7.85 (d, J = 8.5 Hz, 2H), 7.56 – 7.46 (m, 3H), 7.41 – 7.34 (m, 3H), 7.16 (dt, J = 28.0, 7.5 Hz, 2H), 7.04 (d, J = 8.8 Hz, 2H), 5.15 (s, 2H), 4.70 (d, J = 5.6 Hz, 2H), 4.25 (t, J = 7.6 Hz, 2H), 3.95 (q, J = 7.1 Hz, 2H), 2.32 (t, J = 7.3 Hz, 3H), 1.92 (p, J = 7.4 Hz, 2H), 1.08 (t, J = 7.1 Hz, 3H).

Compound 4d: White powder, yield 76%, m. p. 140-141 °C. FT-IR (ATR; 1/ λ, cm^{-1}): 3286 (N-H secondary amide), 3040 (CH aromatic), 1720 (C=O ester),1624 (C=O amide),1608 (C=N benzimidazole), 1535 and 1504 (aromatic C–C). 1H-NMR (500 MHz, DMSO) : 8.95 (t, J = 5.6 Hz, 1H), 7.87 – 7.81 (m, 2H), 7.52 (t, J = 8.2 Hz, 2H), 7.26 – 7.16 (m, 4H), 7.16 – 7.08 (m, 2H), 7.03 (d, J = 8.4 Hz, 2H), 5.08 (s, 2H), 4.70 (d, J = 5.5 Hz, 2H), 4.25 (t, J = 7.7 Hz, 2H), 3.95 (q, J = 7.1 Hz, 2H), 2.32 (t, J = 7.3 Hz, 2H), 2.27 (s, 3H), 1.92 (p, J = 7.5 Hz, 2H), 1.08 (t, J = 7.1 Hz, 3H).

3.1.5. 4-(2-((4-(benzyloxy)benzamido)methyl)-1H-benzo[d]imidazole-1-yl)butanoic acid derivatives (1e-4e):

Compound 1e: White powder, yield 92%, m. p202-204 °C. FT-IR (ATR; 1/ λ, cm^{-1}):3400-2400 (OH carboxylic acid), 3379 (N-H secondary amide), 3070 (CH aromatic), 1705 (C=O carboxylic acid),1643 (C=O amide),1604 (C=N benzimidazole), 1546 and 1504 (aromatic C–C). 1H NMR (500 MHz, DMSO) δ 12.16 (s, 1H), 8.97 (t, J = 5.6 Hz, 1H), 7.85 (d, J = 8.4 Hz, 2H), 7.52 (t, J = 7.8 Hz, 2H), 7.47 (dd, J = 8.3, 5.5 Hz, 2H), 7.18 (td, J = 8.1, 4.6 Hz, 3H), 7.13 (t, J = 7.5 Hz, 1H), 7.03 (d, J = 8.5 Hz, 2H), 5.10 (s, 2H), 4.70 (d, J = 5.6 Hz, 2H), 4.25 (t, J = 7.7 Hz, 2H), 2.25 (t, J = 7.2 Hz, 2H), 1.89 (p, J = 7.4 Hz, 2H).

Compound 2e: White powder, yield 71%, m. p. 207-209 °C. FT-IR (ATR; 1/ λ, cm^{-1}): 3300-2500 (OH carboxylic acid), 3217 (N-H secondary amide), 3032 (CH aromatic), 1701 (C=O carboxylic acid),1643 (C=O amide),1604 (C=N benzimidazole), 1585 and 1509 (aromatic C–C). 1H NMR (500 MHz, DMSO) δ 12.15 (s, 1H), 8.95 (t, J = 5.6 Hz, 1H), 7.83 (d, J = 8.5 Hz, 2H), 7.52 (t, J = 7.0 Hz, 2H), 7.34 (d, J = 8.3 Hz, 2H), 7.19 (t, J = 7.6 Hz, 1H), 7.13 (t, J = 7.5 Hz, 1H), 7.02 (d, J = 8.6 Hz, 2H), 6.90 (d, J = 8.5 Hz, 2H), 5.03 (s, 2H), 4.70 (d, J = 5.6 Hz, 2H), 4.25 (t, J = 7.6 Hz, 2H), 3.71 (s, 3H), 2.28 – 2.20 (m, 2H), 1.89 (p, J = 7.4 Hz, 2H).

Compound 3e: White powder, yield 90%, m. p223-225 °C. FT-IR (ATR; 1/ λ, cm^{-1}):3300-2500 (OH carboxylic acid), 3268 (N-H secondary amide), 3074 (CH aromatic), 1701 (C=O carboxylic acid),1631 (C=O amide),1608 (C=N benzimidazole), 1543 and 1505 (aromatic C–C). 1H-NMR (500 MHz, DMSO) : 12.15 (s, 1H), 8.97 (t, J = 5.8 Hz, 1H), 7.88 (d, J = 8.5 Hz, 2H), 7.49 (s, 1H), 7.42 – 7.33 (m, 5H), 7.07 (t, J = 7.8 Hz, 4H), 5.16 (s, 2H), 4.62 (d, J = 5.7 Hz, 2H), 3.29 (s, 2H), 3.25 (s, 2H), 2.23 (t, J = 7.4 Hz, 2H).

Compound 4e: White powder, yield 82%, m. p. 190-192 °C. FT-IR (ATR; 1/ λ, cm^{-1}): 3400-2400 (OH carboxylic acid), 3417 (N-H secondary amide), 3090 (CH aromatic), 1708 (C=O carboxylic acid),1654 (C=O amide),1608 (C=N benzimidazole), 1543 and 1504 (aromatic C–C). 1H-NMR (500 MHz, DMSO) : 12.24 (s, 1H), 9.49 (d, J = 5.7 Hz, 1H), 7.96 (d, J = 8.1 Hz, 1H), 7.90 (d, J = 8.5 Hz, 2H), 7.74 (d, J = 7.9 Hz, 1H), 7.54 (dt, J = 19.4, 7.4 Hz, 2H), 7.27 – 7.17 (m, 3H), 7.09 (dd, J = 17.5, 8.0 Hz, 3H), 5.10 (s, 2H), 4.93 (d, J = 4.9 Hz, 2H), 4.51 (t, J = 7.8 Hz, 2H), 2.40 (t, J = 7.3 Hz, 2H), 2.27 (s, 3H), 2.00 (p, J = 7.4 Hz, 2H.

3.1.6. 4-(benzyloxy)-*N*-((1-(4-morpholino-4-oxobutyl)-*1H*-benzo[*d*]imidazole-2-yl) methyl)benzamide derivatives (1f-4f):

(figures 1S-16S supplementary file)

Compound 1f: White powder, yield 25%, m. p57-60°C. FT-IR (ATR; 1/ λ, cm^{-1}): 3267 (N-H secondary amide), 3043 (CH aromatic), 1639 (C=O amide),1604 (C=N benzimidazole), 1534 and 1504 (aromatic C–C), 1111 (C-O-C morpholine). 1H NMR (500 MHz, DMSO) δ 9.16 (t, J = 5.5 Hz, 1H), 8.01 (d, J = 8.4 Hz, 2H), 7.70 (t, J = 8.3 Hz, 2H), 7.62 (dd, J = 8.4, 5.4 Hz, 2H), 7.38 – 7.26 (m, 4H), 7.19 (d, J = 8.5 Hz, 2H), 5.25 (s, 2H), 4.87 (d, J = 5.5 Hz, 2H), 4.41 (t, J = 7.5 Hz, 2H), 3.60 (p, J = 4.7 Hz, 5H), 3.51 (t, J = 4.8 Hz, 3H), 2.46 (t, J = 7.0 Hz, 2H), 2.07 (p, J = 7.1 Hz, 2H).13C NMR (125 MHz, DMSO) δ 170.43, 166.13, 163.27, 161.19, 152.33, 135.62, 133.39, 130.58, 130.51, 129.72, 126.75, 122.60, 122.05, 119.09, 115.85, 115.68, 114.85, 110.72, 69.12, 66.50, 66.43, 45.58, 43.08, 41.92, 36.62, 29.23, 25.22. ESI-Mass (m/z): 531.2 $[M^{+1}]$+, calcd. for: $C_{30}H_{31}FN_4O_4$,530.6.

Compound 2f: White powder, yield 45%, m. p. 119-120°C. FT-IR (ATR; 1/ λ, cm^{-1}): 3213 (N-H secondary amide), 3059 (CH aromatic), 1669 ,1643(C=O amide),1608 (C=N benzimidazole), 1543 and 1504 (aromatic C–C), 1114 (C-O-C morpholine). 1H NMR (500 MHz, DMSO) δ 9.15 (t, J = 5.6 Hz, 1H), 8.02 (d, J = 8.4 Hz, 2H), 7.69 (dd, J = 7.9, 3.7 Hz, 3H), 7.53 (d, J = 5.4 Hz, 2H), 7.31 (dt, J = 28.8, 7.6 Hz, 2H), 7.20 (d, J = 8.4 Hz, 2H), 5.29 (s, 2H), 4.87 (d, J = 5.6 Hz, 2H), 4.40 (t, J = 7.6 Hz, 2H), 3.63 – 3.59 (m, 3H), 3.58 (d, J = 4.5 Hz, 2H), 3.51 (t, J = 4.9 Hz, 3H), 3.42 (t, J = 4.7 Hz, 3H), 2.46 (t, J = 7.0 Hz, 2H), 2.07 (p, J = 7.1 Hz, 2H).^{13}C NMR (125 MHz, DMSO) δ 170.43, 166.09, 161.02, 152.32, 142.50, 139.74, 135.71, 133.61, 130.87, 129.74, 128.33, 127.86, 126.92, 126.71, 122.50, 121.93, 119.21, 114.86, 110.65, 68.88, 66.50, 66.43, 56.51, 45.57, 43.04, 41.92, 39.48, 36.65, 29.23, 25.24. ESI-Mass (m/z): 543.2 $[M^{+1}]$+, calcd. for: $C_{31}H_{34}N_4O_5$, 542.6.

Compound 3f: White powder, yield 75%, m. p 139-141°C. FT-IR (ATR; 1/ λ, cm^{-1}): 3278 (N-H secondary amide), 3090 (CH aromatic), 1647,1627 (C=O amide),1608 (C=N benzimidazole), 1557,1534 and 1505 (aromatic C–C), 1118 (C-O-C morpholine). 1H-NMR (500 MHz, DMSO) : 9.12 (t, J = 5.7 Hz, 1H), 7.99 (d, J = 8.4 Hz, 2H), 7.68 (dd, J = 8.0, 5.0 Hz, 2H), 7.49 (d, J = 8.2 Hz, 2H), 7.33 (t, J = 7.6 Hz, 1H), 7.28 (t, J = 7.6 Hz, 1H), 7.17 (d, J = 8.4 Hz, 2H), 7.05 (d, J = 8.2 Hz, 2H), 5.18 (s, 2H), 4.86 (d, J = 5.6 Hz, 2H), 4.40 (t, J = 7.6 Hz, 2H), 3.59 (p, J = 4.6 Hz, 4H), 3.51 (t, J = 4.8 Hz, 2H), 3.41 (d, J = 4.2 Hz, 2H), 2.45 (t, J = 7.0 Hz, 2H), 2.06 (p, J = 7.1 Hz, 2H. 13C-NMR (125 MHz, DMSO) : 170.42, 166.11, 161.36, 159.55, 152.34, 142.54, 135.72, 130.09, 129.67, 128.97, 126.58, 122.48, 121.91, 119.23, 114.84, 114.32, 110.64, 69.64, 66.50, 66.43, 55.57, 45.57, 43.03, 41.92, 36.64, 29.23, 25.24. ESI-Mass (m/z): 547.2 $[M^{+1}]$+, calcd. for: $C_{30}H_{31}ClN_4O_4$,547.04

Compound 4f: White powder, yield 55%, m. p. 139-200 °C. FT-IR (ATR; 1/ λ, cm^{-1}): 3267 (N-H secondary amide), 3039 (CH aromatic), 1639 (C=O amide),1604 (C=N benzimidazole), 1573,1539 and 1504 (aromatic C–C), 1111 (C-O-C morpholine). 1H-NMR (500 MHz, DMSO) : 8.97 (t, J = 5.6 Hz, 1H), 7.87 – 7.82 (m, 2H), 7.53 (dd, J = 8.1, 4.2 Hz, 2H),

7.26 – 7.15 (m, 4H), 7.15 – 7.07 (m, 2H), 7.03 (d, J = 8.6 Hz, 2H), 5.07 (s, 2H), 4.71 (d, J = 5.5 Hz, 2H), 4.25 (t, J = 7.6 Hz, 2H), 3.48 – 3.41 (m, 4H), 3.36 (d, J = 4.8 Hz, 2H), 3.27 (d, J = 5.3 Hz, 2H), 2.30 (t, J = 6.9 Hz, 2H), 2.27 (s, 3H), 1.92 (p, J = 7.3 Hz, 2H). 13C-NMR (125 MHz, DMSO) : 170.44, 166.13, 161.33, 152.32, 142.56, 138.12, 137.04, 135.72, 129.70, 129.05, 128.85, 128.80, 126.68, 125.34, 122.48, 121.91, 119.24, 114.82, 110.63, 69.88, 66.49, 66.42, 45.58, 43.02, 41.92, 36.64, 29.23, 25.24, 21.45. ESI-Mass (m/z): 527.2 $[M^{+}1]$+, calcd. for: $C_{31}H_{34}N_4O_4$, 526.6.

Scheme 1 illustrates the review of the chemical synthesis of desired compounds (1f-4f) with the 2-(aminomethyl)benzimidazole nucleus, in which all the synthesized compounds were started with Williamson ether synthesis by the reaction of different substituted benzyl bromide derivatives and ethyl 4-(hydroxy)benzoate resulting in ester compounds (1a - 4a). These compounds were hydrolyzed under alkaline conditions to yield the corresponding carboxylic acid derivatives (1b-4b). [38-39]

N-acylation of the reactive primary amine of 2-(aminomethyl)benzimidazole by aromatic carboxylic acid (1b-4b) was facilitated by the addition of the coupling agent N-Ethyl-N′-(3-dimethylaminopropyl)carbodiimide hydrochloride (EDC.HCl) with 1-hydroxy benzotriazole (HOBt) as a nucleophile in an aprotic solvent. The reaction involves many steps:

1st: O-acyl isourea formation (nucleophilic addition of N-carbodiimide to the carbonyl group)

2nd: The intermediate is racemized to unreactive N-acyl urea

3rd: HOBt which is a strong nucleophile reacts faster than the competing acyl transfer and generates an activated ester

4th: Aminolysis; is facilitated by the reactive electrophilic property of the activated ester and the strong nucleophilic property of the aliphatic primary amine.

The reaction must be done in polar aprotic solvents, which do not solvate the nucleophile since no ionization occurs, making the latter free to be attacked by an electrophile. [40-42]

The slightly basic nitrogen of benzimidazole needs to be activated by a basic condition (anhydrous K_2CO_3) that can abstract the proton, leaving the nitrogen with an unshared pair of electrons as a nucleophile to attack ethyl-4-bromobutanoate, which is treated with KI before its addition to replace the bromide ions by an iodide ion, which has a better leaving property [43] resulting in the N alkylation of benzimidazole.

1d – 4d compounds were hydrolyzed in basic medium to their corresponding carboxylic acids, then these acids were reacted with morpholine by N acylation, which is facilitated by the addition of TEA as a base and DMAP as an acetyl transferase agent, which is added to proceed the reaction through the acyliminum ion intermediate more efficiently. [32]

The progression of each reaction step had been confirmed, and each resulting compound was subjected to many physical and advanced analytical methods. All the results indicate precise and pure compounds, as mentioned above and supported by figures (1S–16S) in the supplementary file.

3.2. Invitro cytotoxic study: For cytotoxic studies against two cancer cell lines—human breast cancer cells (T47D) and human alveolar cell carcinoma (A549)—as well as Vero normal cells, all of the proposed compounds were evaluated along with gefitinib (as a reference). Both 3f and 4f compounds gave approximately similar cytotoxic effects against human breast cancer cells (T47D) cell lines with IC50 50±5.5 μM and 50.5±3.2μM, respectively, but not more than gefitinib, which had IC_{50} of 21.05 μM. All chemicals showed negligible toxicity in the lung cancer cell line (A549), with the exception of 4f, which had an IC50 of 166.1±92. The cell demonstrated significant resistance to gefitinib, even at concentrations greater than 200μM. Interestingly, all compounds were not cytotoxic against normal cells. The results of IC_{50} are demonstrated in **Table 1**, and the comparison of the cell survival of cytotoxic compounds are represented by **Figures, 3** and **4**. The morphologies of the A549 cell line upon treatment with 4f and gefitinib are shown in **Figure 5**.

As with most lung cancer cell lines, high expression of the EGFR protein is present in A549 [8], but they showed resistance to approximately all com-

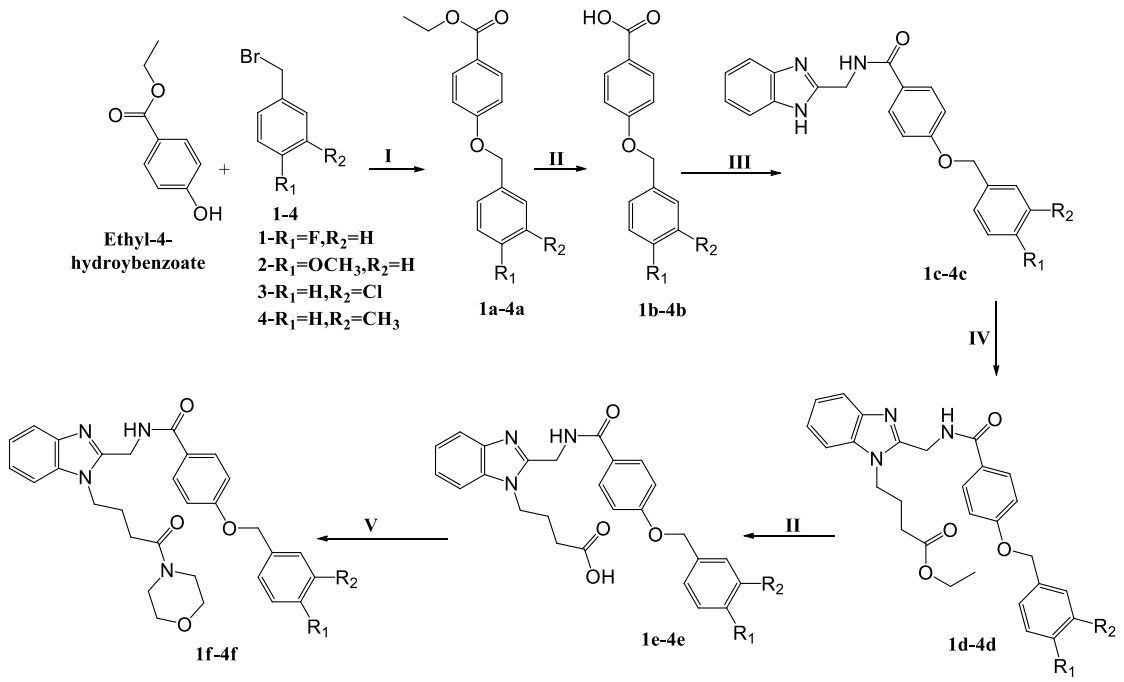

I:anhydrous K_2CO_3,acetoitrile, reflux. II:NaOH. III:EDC, HOBt,DMF,2-aminomethyl benzimidazole. IV:1-anhydrous K_2CO_3 2-KI +Ethyl 4-bromobutanoate. V:EDC, HOBt,TEA,DMAP,morpholine.

Scheme 1: *Synthesis of compounds 1f - 4f*

pounds, even gefitinib. This resistance may be due to the presence of downstream enzyme mutations like the KRAS (Kirsten Rat Sarcoma Viral Oncogene Homolog) mutation or may be due to amplification of HER2 that increases the abundance of ErbB2 protein.[4,44] This may complicate the understanding of the mechanism by which our compounds are working, especially when compared with a clinically approved EGFR TKI, gefitinib.

The breast cancer cell line, T47D, is classified as an estrogen receptor positive (ER^+) breast cancer cell with low expression of the HER2 receptor protein. However, some studies showed an expression of EGFR in ER+ breast cancer cell lines. [45-46] So, the EGFR TKIs may be combined with hormonal therapy for ER-positive metastatic disease. [47] Only 3f and 4f shown a minor cytotoxicity against the breast cancer cell line in our investigation, while gefitinib had a cytotoxic effect on the T47D cell line but more significantly than the other chemicals evaluated.

Additional research was conducted to examine the morphology of the A549 cell line using gefitinib and the 4f molecule. 4f shown a clear reduction in proliferation as compared to the control and gefitinib groups.

As demonstrated by the cytotoxicity of compounds 3f and 4f in a breast cancer cell line, the structure-activity relationship suggests that compounds with meta substitution in the aromatic hydrophobic back pocket are more active than compounds with para substitution. It is more likely that the 4f compound, which has meta methyl substitution, will exhibit dual cytotoxic activity against lung and breast cancer cell lines.

3.3. Docking Study:

In order to get a preliminary confirmation about the enzyme inhibition mode of our synthesized compounds, all compounds are docked with 2 model proteins of RTKs (EGFR, 3POZ and HER2, 3RCD)

Table 1. Cytotoxic activity of the designed compounds against cancerous and normal cells

Compound	T47D	A549	Vero
	IC_{50}*	IC_{50}*	IC_{50}*
1f	>200	>200	>200
2f	187±16.6	>200	>200
3f	50±5.5	>200	>200
4f	50.5±3.2	166.1±92	>200
Gefitinib	21.05±2.15	>200	>200

*All calculated IC_{50} are in μM

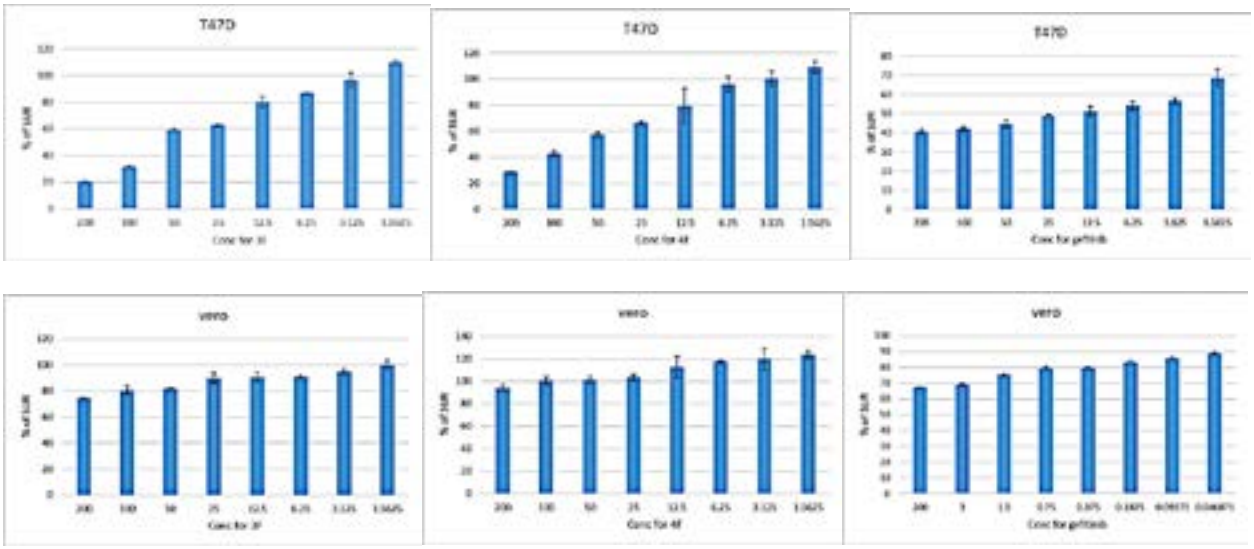

Figure 3: *Antiproliferative effect of* ***3f,4f*** *and* ***gefitinib*** *against T47D and Vero normal cell lines*

downloaded from PDB (www.rcsb.org). The docking scores represented by binding free energy with calculated Ki as well as RMSD are summarized in **Table 2**. The 2D and 3D interactions with binding sites are shown in figures 17S-25S (supplementary file).

The redocking results of the original co-crystallized ligand (TAK-285) with two selected proteins (3POZ; EGFR and 3RCD; HER2) were (ΔG -9.2, RMSD 1.4 and ΔG -9.3, RMSD 1.6) respectively, which indicate a good docking process.

As it is known, the small ΔG value, indicates a good interaction between the protein and the ligand. The RMSD near 1 and less than 2 means that the ligand fits well with the reference recrystallized ligand within the binding pocket.48 According to the results that are mentioned in table 2, all the binding

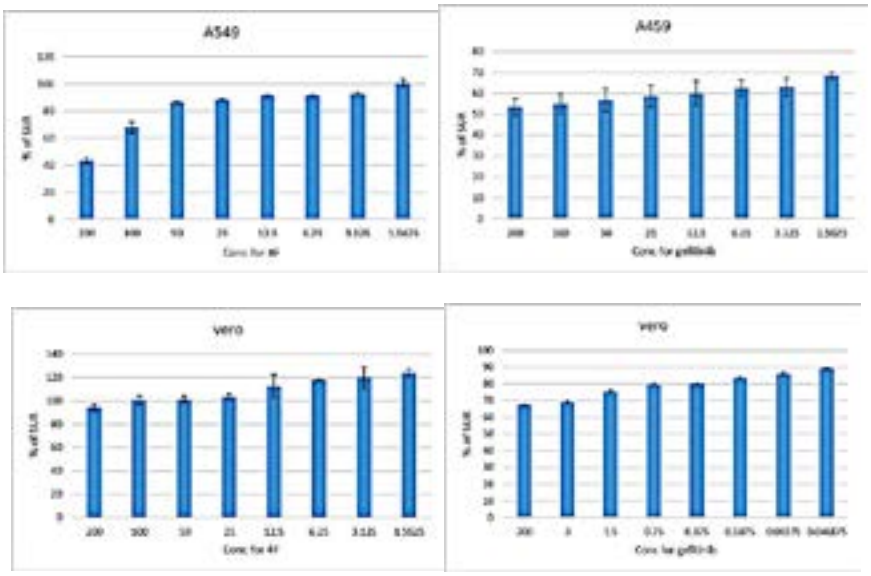

Figure 4: *Antiproliferative effect of* ***4f*** *and* ***gefitinib*** *against A549 and Vero normal cell lines*

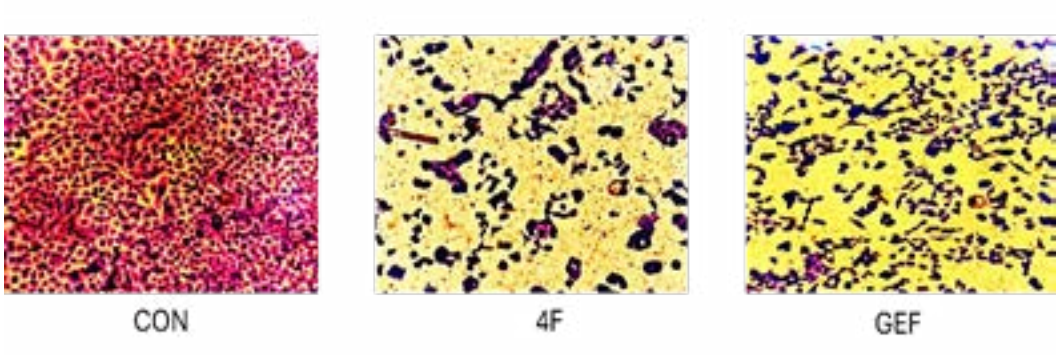

Figure 5: *Morphology of the A549 after treatment with compound 4f and gefitinib at the* IC_{50} *with control*

energies with corresponding inhibitory constants are better than gefitinib. However, only (4f) exhibits superior ΔG and RMSD values when compared to gefitinib, but only in the 3POZ protein, indicating its efficacy against the highly resistant lung cancer cell line (A549) that expresses high levels of EGFR.

The 2D and 3D interactions of the synthesized ligands with gefitinib within the protein ligand binding pockets are shown in Figures 17S and 21S; supplemental file. In these figures, the most important amino acid residues for the interaction of TAK-285 with the (EGFR, 3POZ) protein are MET793, LYS745, 6-ring PHE856, LEU788, and VAL 726, which appear as assigned residues in 2D modes. For the tested compounds, the amino acid residues were GLY719 with 1f, GLY719 and VAL 726 with 2f, and LYS745 with 4f, while 3f showed no interaction with the binding site. The other protein (HER2, 3RCD); as in figures (22S-26S) supplementary file, the amino acids that interact with TAK-285 are ASP863, LYS753, ASN850, and MET 801. For the other tested compounds, only 1f and

Table 2. Docking results of the designed compounds with both EGFR and HER2

Compound	EGFR, 3POZ			HER2, 3RCD		
	ΔG(kcal/mol)	RMSD*	Ki(μM)	ΔG(kcal/mol)	RMSD	Ki(μM)
1f	-9	2.9	0.19	-7.9	2.2	0.55
2f	-8.4	3	0.3	-8.1	4	0.51
3f	-7.7	3.8	0.76	-7.7	4.3	0.76
4f	-8.9	1	0.2	-9.2	2.8	0.17
Gefitinib	-7.6	0.9	0.8	-8.1	1.8	0.51

* RMSD, root mean square deviation of a ligand with respect to the reference conformation

Table 3a: SwissADME descriptors of 4f and gefitinib

Compound	Formula	MW	#H-bond acceptors	#H-bond donors	TPSA*Å^2	ESOL Class
4f	$C_{31}H_{34}N_4O_4$	526.63	5	1	85.69	Moderately soluble
Gefitinib	$C_{22}H_{24}ClFN_4O_3$	446.90	7	1	68.74	Moderately soluble

*Topological Polar Surface Area

Table 3b: SwissADME descriptors of 4f and gefitinib

Compound	Consensus Log P	GI absorption	BBB permeant	Lipinski #violations	Bioavailability Score
4f	3.83	High	No	1	0.55
Gefitinib	3.86	High	Yes	0	0.55

4f showed interaction in the binding pocket with the amino acids GLY727 and THR862, ASP863, respectively. It is worth noting that gefitinib has no interaction with the (EGFR, 3POZ) pocket while interacting with ALA730 and VAL734 in the (HER2, 3RCD) binding pocket.

3.4. Molecular Dynamic Simulation:

The Simulation Interactions Diagram Reports cover analysis of protein-ligand Root Mean Square Deviation (RMSD), protein Root Mean Square Fluctuation (RMSF), protein secondary structure, ligand RMSF, protein-ligand contacts and ligand

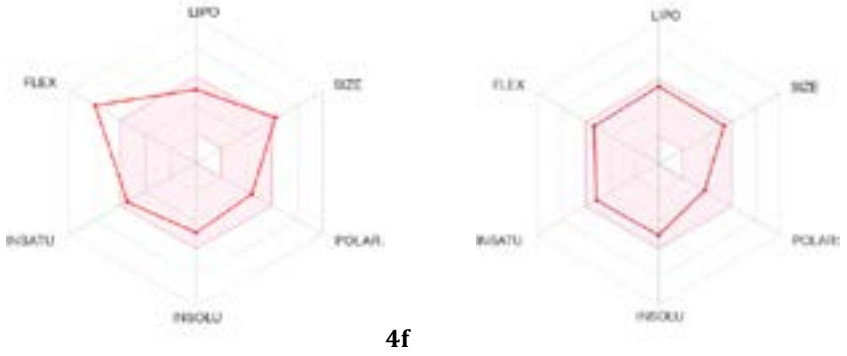

4f **gefitinib**

Figure 6: *Bioavailability radars of 4f and gefitinib: The pink area represents the range of the optimal property values for oral bioavailability and the red line is compound 4f predicted properties. Saturation (INSATU), size (SIZE), polarity (POLAR), solubility (INSOLU), lipophilicity (LIPO) and flexibility (FLEX).*

properties, which are all illustrated in figures (27S and 28S) in the supplementary file. [49]

Unlike the more static molecular docking method, MD modeling does not ignore the fact that proteins change over time,[36] so for more confirmation about the pharmacological activity of the high cytotoxic compound (4f) on both T47D and A549 cell lines, MDS was done with both 3RCD and 3POZ proteins.

MDS predicts how every atom in a protein or other molecular system will move over time, based on a general model of the physics governing interatomic interactions. Also, these simulations capture the behavior of proteins and other biomolecules in full atomic detail and at very fine temporal resolution.[50]

The protein conformational change was explained by the difference in the position of the Cα atoms of the protein backbone and was reported in Å and plotted as a function of simulation time, as in figures (27S-a and 28S-a) in the supplementary file. The RMSD of the 4f- 3POZ complex was approximately 2.4, which is considered acceptable for this protein while there was a higher RMSD of the 4f- 3RCD complex (approximately 12).

The Root Mean Square Fluctuation (RMSF) is useful for characterizing local changes along the protein chain. Secondary structure elements like alpha helices and beta strands are usually more rigid than the unstructured part of the protein, and thus fluctuate less than the loop regions, while the tails (N- and C-terminal) fluctuate more than any other part of the protein. As seen in figures (27S-b and 28S-b), a narrow range of RMSF values of the active site residues of the complexes, marked with green-colored vertical bars, demonstrates that these compounds are capable of forming stable interactions with the protein during MDS.

The Ligand Root Mean Square Fluctuation (L-RMSF) is useful for characterizing changes in the ligand atom positions. The ligand RMSF may give us insights on how ligand fragments interact with the protein and their entropic role in the binding event. Ligand RMSF shows the ligand's fluctuations broken down by atom, the more stable the ligand, the less fluctuation will be observed, and in the 4f-3POZ complex (Figure 27S-c), little fluctuation is present between 32 and 36 atoms, as shown in the 2D structure, which may be due to the lake of hydrogen bonding at this part of the molecule. In figure 28S-c of the 4f-3RCD complex, more fluctuation was demonstrated.

Protein interactions with the ligand can be monitored throughout the simulation. These interac-

tions can be categorized by type and summarized in figures (27S-d&e and 28S-d&e), which represent the interactions that occur in more than 30% of the simulation time in the selected trajectory (0.00 through 20 and 50.05 nsec, respectively).

In the 4f-3POZ complex, the most important interaction was the hydrogen bond of the oxygen atom of the carbonyl group of the secondary amide with THR790, the gatekeeper of the ATP binding pocket, while in the 4f-3RCD complex, the hydrogen bonding of the oxygen atom of morpholine with MET801 (one of the important amino acid residues that interact with most TKIs).

3.5. ADME study:

Only compound 4f, with valuable cytotoxic activity and good molecular modeling results, was subjected to study for its pharmacokinetic properties compared with gefitinib, as shown in **Table 3**. Also, the bioavailability radar enables a first glance at drug likeness (**Figure 6)**.

According to the Swiss ADME descriptor data, **Table 3**, and upon comparison with gefitinib (FDA-approved TKI), the 4F compound has good drug likeness, which is represented by Lipinski rules. Only the molecular weight is a little more than 500, but others, like H-bond donners with no more than 5, H-bond acceptors with no more than 10, and log p with less than 5. The topological surface area conflicts with high GI absorption (less than 140 ºA2), but no brain permeability presents (more than 80).[37,51] Interestingly, the 4F compound has the same bioavailability as gefitinib (0.55), which makes it a more acceptable candidate for further in vitro and in vivo studies.

Figure 6 shows the bioavailability radar, in which the pink area represents the optimal range with different parameters, and with the 4F compound, only the flexibility parameter shows a little deviation from the boundary lines.

4. Conclusion

All proposed compounds with intermediates were effectively synthesized in pure forms, based on the results of the advanced chemical analysis. Compound 4f had a greater antiproliferative effect than reference in the cytotoxic study when applied to the A549 lung cancer cell line, which exhibited high resistance to all other compounds. The T47D breast cancer cell line was equally susceptible to the cytotoxicity of compounds 3f and 4f, but not more so than gefitinib. Good results with compound 4f and a good ligand interaction model were shown by the docking investigation. Stable structural changes were seen by the MDS along the chosen paths, particularly with the EGFR protein (3POZ). The ADME research demonstrated high bioavailability and drug similarity. Thus, in order to be taken into consideration as a dual EGFR/HER2 TKI, compound 4f is thought to be a suitable candidate for more structural optimization and biological research.

ABBREVIATIONS: *(RTK) Receptor tyrosine kinase; (ADME) absorption, distribution, metabolism, and elimination; (TKI) tyrosine kinase inhibitor; (HER2) human epidermal growth factor receptor-2; (EGFR) Epidermal growth factor receptor; (PKIs) Protein kinase inhibitor; (IR) Infrared Radiation; (NMR) Nuclear Magnetic Resonance; (MS) Mass spectrum; (IC50) Half-Maximal Inhibitory Concentration; (PDB) Protein Data Bank; (MOE) Molecular Operating Environment; (EDC.HCl) 1-ethyl-3-(3'-dimethylamino) carbodiimide HCl; (HOBt) N-hydroxy benzotriazole; (DMAP) dimethyl amino pyridine; (DMF) Dimethylformamide; (RMSD) root mean square deviation; (RMSF) Root Mean Square Fluctuation; (MDS) Molecular Dynamic Simulation; (MW) molecular weight; (TPSA) Topological surface area; (ESOL) estimated solubility; (GI) gastro intestinal; (BBB) blood brain barrier; (INSATU) Saturation; (POLAR) polarity; (INSOLU) solubility; (LIPO) lipophilicity; (FLEX) flexibility; (KRAS) Kirsten Rat Sarcoma Viral Oncogene Homolog.*

ACKNOWLEDGMENT
The authors are thankful to university of Baghdad,

college of pharmacy, Department of Pharmaceutical Chemistry, for providing chemicals and research facilities to carry out the work, the authors are also thankful to university of Jorden for spectral characterization (NMR and MS) of compounds and to Applied Science Private University for cytotoxic study.

Conflicts of Interest

The authors declare no conflicts of interest.

Funding

This research received no external funding.

Ethics Statement

The authors did not use animals in the study

Author Contribution

Conceptualization and supervision, M.H.M.; investigation, methodology, and manuscript writing, S.Q. Al-S.; Cytotoxic methodology, W.H.T.

References

1- Debela D.T., Muzazu S.G., Heraro K.D., Ndalama M.T., Mesele B.W., Haile D.C., Kitui S.K., Manyazewal T. New approaches and procedures for cancer treatment: Current perspectives. *SAGE Open Med*. 12, 9, 2021. https://doi.org/10.1177/20503121211034366

2- Abdulrahman H.S., Mohammed H.M., Al-Ani L.A., Ahmad M.H., Hashim N.M., Yehye W.Y. Synthesis of Phthalimide Imine Derivatives as a Potential Anticancer Agent. *J. Chem.* 3928204, 13 pages, 2020 https://doi.org/10.1155/2020/3928204

3- Sagheer O.M., Mohammed M.H., Ibraheem Z.O., Wadi J.S., Tawfeeq M.F. Synthesis of gamma biguanides butyric acid analogues as HDAC inhibitors and studying their cytotoxic activity. *Mater. Today Proc*. 47, 17, 5983-5991, 2021. https://doi.org/10.1016/j.matpr.2021.04.539

4- Bansal I., Pandey A.K., Ruwali, M. Small-molecule inhibitors of kinases in breast cancer therapy: recent advances, opportunities, and challenges. *Front. Pharmacol*. 14, 1244597, 2023. https://doi.org/10.3389/fphar.2023.1244597

5- Murthy R. K., Loi S., Okines A., Paplomata E., Hamilton E., Hurvitz S. A., Lin N.U., *et al*. Tucatinib, Trastuzumab, and Capecitabine for HER2-Positive Metastatic Breast Cancer. *N. Engl. J. Med*. 382, 7, 597–609, 2020. doi: 10.1056/NEJMoa1914609

6- Sigismund S., Avanzato D., Lanzetti L. Emerging functions of the EGFR in cancer. *Mol. Oncol*. 12, 3–20, 2018. https://doi.org/10.1002/1878-0261.12155

7- Saraon P., Pathmanathan S., Snider J., Lyakisheva A., Wong V., Stagljar I. Receptor tyrosine kinases and cancer: oncogenic mechanisms and therapeutic approaches. *Oncogene*. 40, 4079–4093, 2021. doi: https://doi.org/10.1038/s41388-021-01841-2

8- Ayatia A., Moghimia S., Salarinejadb S., Safavic M., Pouramiria B., Foroumadia A. A review on progression of epidermal growth factor receptor (EGFR) inhibitors as an efficient approach in cancer targeted therapy. *Bioorg. Chem*. 99, 103811, 2020. https://doi.org/10.1016/j.bioorg.2020.103811

9- Abdulkhaleq Z.M., Mohammed M.H. Molecular Docking, Synthesis, characterization and preliminary cytotoxic evaluation of new 1, 3,4-Thiadiazole derivatives as EGFR Inhibitors. *Mater. Today Proc.* 65, 249-250, 2022. https://doi.org/10.1016/j.matpr.2022.04.315

10- Yang Y., Li S., Wang Y., Zhao Y., Li Q. Protein tyrosine kinase inhibitor resistance in malignant tumors: molecular mechanisms and future perspective. *Signal Transduct. Target. Ther.* 7, 329, 2022. https://doi.org/10.1038/s41392-022-01168-8

11- Niederst, M. J., & Engelman, J. A. Bypass mechanisms of resistance to receptor tyrosine kinase inhibition in lung cancer. *Sci. signal.* 6, 294, re6, 2013. https://doi.org/10.1126/scisignal.2004652

12- Bertoli E., De Carlo E., Del Conte A., Stanzione B., Revelant A., Fassetta K., Spina M., Bearz A.

Acquired Resistance to Osimertinib in *EGFR*-Mutated Non-Small Cell Lung Cancer: How Do We Overcome It? *Int. J. Mol. Sci.* 23, 13, 6936, 2022. https://doi.org/10.3390/ijms23136936

13-Bhatia P., Sharma V., Alam O., Manaithiya A., Alam P., Kahksha, Alam M.T., Imran M. Novel quinazoline-based EGFR kinase inhibitors: A review focussing on SAR and molecular docking studies (2015-2019). *Eur. J. Med. Chem.* 204, 112640, 2020. https://doi.org/10.1016/j.ejmech.2020.112640

14-Guo T., Ma S. Recent Advances in the Discovery of Multitargeted Tyrosine Kinase Inhibitors as Anticancer Agents. *ChemMedChem.* 16, 4, 600-620, 2021. https://doi.org/10.1002/cmdc.202000658

15-Li M., Rehman A.U, Liu Y., Chen K., Lu S. (2021). Dual roles of ATP-binding site in protein kinases: Orthosteric inhibition and allosteric regulation, In: Donev, R. eds. Protein Kinases in Drug Discovery. Advance in protein chemistry and structural biology, Elsevier, MicroPharm Ltd, United Kingdom, 87-119. https://doi.org/10.1016/bs.apcsb.2020.09.005

16-Milik S.N., Lasheen D.S., Serya R.A.T., Abouzid K. A.M. How to train your inhibitor: Design strategies to overcome resistance to Epidermal Growth Factor Receptor inhibitors. *Eur.J.Med.Chem.* 142, 131-15, 2017. https://doi.org/10.1016/j.ejmech.2017.07.023

17- Fakhry M.M., Mattar A.A., Alsulaimany M., Al-Olayur,an E.M., Al-Rashood S.T., Abdel-Aziz H.A. New Thiazolyl-Pyrazoline Derivatives as Potential Dual EGFR/HER2 Inhibitors: Design, Synthesis, Anticancer Activity Evaluation and *In Silico* Study. *Molecules* 28, 21, 7455, 2023. https://doi.org/10.3390/molecules28217455

18-Elwaie T.B., Abbas S.E., Aly E.I., El Sayed R.K., Abd Elmageed Z.Y., Ali H.I. HER2 Kinase-Targeted Breast Cancer Therapy: Design, Synthesis, and *In Vitro* and *In Vivo* Evaluation of Novel Lapatinib Congeners as Selective and Potent HER2 Inhibitors with Favorable Metabolic Stability. *J. Med. Chem*. 63, 24, 15906–15945, 2020. https://doi.org/10.1021/acs.jmedchem.0c01647

19-Şandor A., Ionuț I., Marc G., Oniga I., Eniu D., Oniga O. Structure–Activity Relationship Studies Based on Quinazoline Derivatives as EGFR Kinase Inhibitors (2017–Present). *J. Pharm.* 16, 4,534, 2023. https://doi.org/10.3390/ph16040534

20-Nadhum S.A., Kamoon R.A., Mohammed H.M. 6-Mercaptopurine derivatives: maintenance therapy of acute lymphoblastic leukemia: A review. *Biochem. Cell. Arch*. 20, 1, 2091-2099, 2020. https://connectjournals.com/file_html_pdf/3146801H_2091A.pdf.

21-Abdullah M.N., Hamid S.A., Salhimi S.M., Jalil N.A., Al-Amin M., Jumali NS. Design and synthesis of 1sec/tertbutyl-2-chloro/nitrophenyl benzimidazole derivatives: Molecular docking and in vitro evaluation against MDA-MB-231 and MCF-7 cell lines. *J. Mol. Struct.* 1277, 13428, 2023. https://doi.org/10.1016/j.molstruc.2022.134828

22-Haider K., Shahar Yar M. (2022). Advances of Benzimidazole Derivatives as Anticancer Agents: Bench to Bedside. Biochemistry. *IntechOpen*. http://dx.doi.org/10.5772/intechopen.101702

23-Abd El-Meguid E.A., Mohi El-Deen E.M., Nael M.A., Anwar M.M. Novel benzimidazole derivatives as anti-cervical cancer agents of potential multi-targeting kinase inhibitory activity. *Arab.J.Chem.* 13, 9179-9195, 2020. https://doi.org/10.1016/j.arabjc.2020.10.041

24-Lee Y.T., Tan Y.J., Oon C.E. Benzimidazole and its derivatives as cancer therapeutics: The potential role from traditional to precision medicine. *Acta Pharm. Sin. B.*13, 2, 478-497, 2023. Available in: https://doi.org/10.1016/j.apsb.2022.09.010

25-Abdulkhaleq Z.M., Mohammed M.H. Molecular docking, synthesis, characterization, and preliminary cytotoxic evaluation of new 1,3,4-thiadiazole derivatives as alpha- estrogen receptor modulator. *J. Contemp. Med. Sci.* 8, 3,194-202, 2022. https://doi.org/10.22317/jcms.v8i3.1224

26-Arrata I., Grison C.M., Coubrough H., Prabhakaran P., Little M.A., Tomlinson D.C, Webb M.E., Wilson A.J. Control of Conformation in α-Helix Mimicking Aromatic Oligoamide Foldamers Through Interactions Between Adjacent Side-Chains. *Org. Biomol. Chem*. 17, 3861-3867, 2019. https://doi.org/10.1039/C9OB00123A

27-Jabbar S.S., Mohammed M.H. Design, Synthesis, Insilco Study and Biological Evaluation of New Coumarin-Oxadiazole Derivatives as Potent Histone Deacetylase Inhibitors. *Egypt. J. Chem*. 66, 385-393, 2023. Doi:10.21608/EJCHEM.2022.134043.5912

28-Wennas O.W., Mohammed H.M., Al Abood R.M., Abed D.A. Design, Synthesis, and Biological Evaluation of Camptothecin Loaded Biotinylated Cellulose Nanowhiskers as Anticancer Agents. *J Contemp Med Sci*. 7, 3,145-151, 2021. DOI: https://doi.org/10.22317/jcms.v7i3.960

29-Talib A.B., Mohammed H.M. Preparation, characterization and preliminary cytotoxic evaluation of 6-mercaptopurine-coated biotinylated carbon dots nanoparticles as a drug delivery system. *Mater. Today Proc.* 80, 3, 2327-2333, 2023. https://doi.org/10.1016/j.matpr.2021.06.341

30-Abdel-Latif E., Fahad M.M., Ismail M.A. Synthesis of N-aryl 2-chloroacetamides and their chemical reactivity towards various types of nucleophiles. *Synth. Commun*. 50, 3, 289-314, 2019. https://doi.org/10.1080/00397911.2019.1692225

31-Wang S., Guan L., Zang J., Xing K., Zhang J., Liu D., Zhao L. Structure-Based Design of Novel Benzimidazole Derivatives as Pin1 Inhibitors. *Molecules* 24, 1198, 2019. https://doi.org/10.3390/molecules24071198

32-Ghosh A.K., Shahabi D. Synthesis of amide derivatives for electron deficient amines and functionalized carboxylic acids using EDC and DMAP and a catalytic amount of HOBt as the coupling reagents. *Tetrahedron Lett.* 19, 63, 152719, 2021. https://doi.org/10.1016/j.tetlet.2020.152719

33-Hamed R.A., Talib W.H. Targeting cisplatin resistance in breast cancer using a combination of Thymoquinone and Silymarin: an in vitro and in vivo study. *Pharmacia.* 71, 1-19, 2024. https://doi.org/10.3897/pharmacia.71.e117997

34-Al-Amily D.H., Hassan M. Design, Synthesis, and Docking Study of Acyl Thiourea Derivatives as Possible Histone Deacetylase Inhibitors with a Novel Zinc Binding Group. *Sci. Pharm.* 87, 28, 2019. https://doi.org/10.3390/scipharm87040028

35-Pandey A.K., Verma S. An in-silico evaluation of dietary components for structural inhibition of SARS-Cov-2 main protease. *J. Biomol. Struct. Dyn.* 40, 1, 136-142, 2020. https://doi.org/10.1080/07391102.2020.1809522

36-Hasan Y., Al-hamashi A. Identification of Selisistat Derivatives as SIRT1-3 Inhibitors by in Silico Virtual Screening. *Turk. Comput. Theor. Chem.* 8, 2, 1-11, 2023. https://doi.org/10.33435/tcandtc.1224592

37-Daina A., Michielin O., Zoete V. SwissADME: a free web tool to evaluate pharmacokinetics, drug-likeness and medicinal chemistry friendliness of small molecules. Nature. *Sci. Rep*. 7, 42717, 2017. https://doi.org/10.1038/srep42717

38-Ouellette R.J., Rawn D. (2014). 16-Ethers, and Epoxide. In: Organic Chemistry. Elsevier, 277-297. https://doi.org/10.1016/B978-0-12-800780-8.00016-4

39-Cary F.C., Sundgurg R.J. (2000). Part A: structure and mechanism, reaction of carbonyl compounds. In: Advanced organic chemistry,4th edition; Springer Science+Business Media, LLC, US. 489-508. https://doi.org/10.1007/0-306-46856-5_8

40-Montalbetti C., Falque V.M. Amide bond formation and peptide coupling. *Tetrahedron*: 61, 10827–10852, 2005. https://doi.org/10.1016/j.tet.2005.08.031

41-Valeur E., Bradley M. Amide bond formation: beyond the myth of coupling reagents. *Chem. So.c Rev.* 38, 606–631, 2009. DOI: https://doi.org/10.1039/B701677H

42-Chan L.C., Cox B.G. Kinetics of Amide Formation through Carbodiimide/N-Hydroxybenzotriazole (HOBt) Couplings. *J. Org. Chem*. 72, 8863-8869, 2007. https://doi.org/10.1021/jo701558y
43-Mastitski A., Abramov A., Kruve A., Järv J. Potassium iodide catalysis in the alkylation of protected hydrazines. *P. Est. Acad. Sci.* 66, 1, 10–17, 2017. https://doi.org/10.3176/proc.2017.1.03
44-Wheeler D.L., Dunn E.F., Harari P.M. Understanding resistance to EGFR inhibitors—impact on future treatment strategies. *Nat. Rev. Clin. Oncol.* 7, 493–507, 2010. https://doi.org/10.1038/nrclinonc.2010.97
45-Al-Warhi T., El Kerdawy A.M., Said M.A., Albohy A., Elsayed Z.M., Aljaeed N., Elkaeeb E.B., Eldehna W.M., Abdel-Aziz H.A., Abdelmoaz M.A. Novel 2-(5-Aryl-4,5-Dihydropyrazol-1-yl) thiazol-4-One as EGFR Inhibitors: Synthesis, Biological Assessment and Molecular Docking Insights. *Drug Des. Devel. Ther.* 16, 1457-1471, 2022. https://doi.org/10.2147/DDDT.S356988
46-Johnston S.R.D., Dowsett M. Aromatase inhibitors for breast cancer: lessons from the laboratory. *Nat. Rev. Cancer*. 3, 821-831, 2003. https://doi.org/10.1038/nrc1211
47-Johnston S.R.D. Enhancing the efficacy of hormonal agents with selected targeted agents. *Clin. Breast Cancer*. 9, 1, S28-S36, 2009. doi: 10.3816/CBC.2009.s.003
48-Pantsar T., Poso A. Binding Affinity via Docking: Fact and Fiction. *Molecules*. 23, 1899, 2018. https://doi.org/10.3390/molecules23081899
49-Shaw D. E. (2021) In: Research, Desmond Molecular Dynamics System, New York, NY, Maestro-Desmond Interoperability Tools, Schrödinger, New York, NY (2021).
50-Hollingsworth S. A., Dror R. O. Molecular dynamics simulation for all. *Neuron.* 99, 6, 1129-1143, 2018. https://doi.org/10.1016/j.neuron.2018.08.011
51-Daina A., Zoete V. A BOILED-Egg to Predict Gastrointestinal Absorption and Brain Penetration of Small Molecules. *ChemMedChem.* 11, 1117–1121, 2016. https://doi.org/10.1002/cmdc.201600182